Powder Technology 436 (2024) 119471

Contents lists available at ScienceDirect

Powder Technology

journal homepage: www.journals.elsevier.com/powder-technology

Characterisation of gas-atomised metal powders used in binder jet 3D printing

Wenguang Nan [1], Mehrdad Pasha [2], Umair Zafar [3], Sadegh Nadimi [4], Wei Pin Goh, Mojtaba Ghadiri [*]

School of Chemical and Process Engineering, University of Leeds, Leeds LS2 9JT, UK

HIGHLIGHTS

- Gas-Atomised Metal Powder has been characterised for use in Binder Jet 3D printing.
- Powder flowability and spreadability are assessed by experiment and DEM simulation.
- Flow classification using bulk characterisation tests shows contradictory outcomes.
- Spreadability data does not exhibit strong correlation with bulk powder properties.
- Flowability may not necessarily serve as an accurate measure of spreadability.

GRAPHICAL ABSTRACT

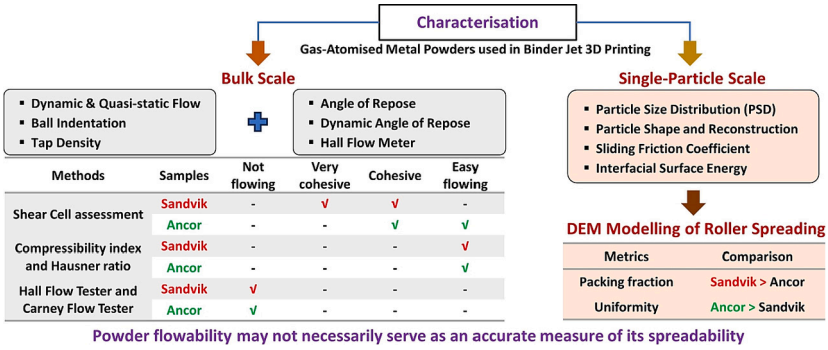

Methods	Samples	Not flowing	Very cohesive	Cohesive	Easy flowing
Shear Cell assessment	Sandvik	-	√	√	-
	Ancor	-	-	√	√
Compressibility index and Hausner ratio	Sandvik	-	-	-	√
	Ancor	-	-	-	√
Hall Flow Tester and Carney Flow Tester	Sandvik	√	-	-	-
	Ancor	√	-	-	-

Metrics	Comparison
Packing fraction	Sandvik > Ancor
Uniformity	Ancor > Sandvik

ARTICLE INFO

Keywords:
Additive manufacturing
Binder jetting
Flowability
Spreadability

ABSTRACT

A comprehensive characterisation study has been undertaken to examine the flowability and spreadability of two distinct types of gas-atomised metal powders used in Binder Jet 3D printing technology. The experimental characterisation encompasses an analysis of the physical properties of individual particles as well as the flow behaviour of bulk powder. The data gathered from individual particle analysis are subsequently employed in numerical simulations of roller spreading by Discrete Element Method (DEM) to gain valuable insights into the intricate interplay between powder attributes and its spreading characteristics. The findings reveal that employing bulk characterisation tests, such as shear cell tests and compressibility indices, results in contradictory outcomes. Moreover, the spreadability data derived from the DEM simulations do not exhibit a strong correlation with the results obtained from the characterisation of the bulk powder. These results underscore that the flowability of the powder may not necessarily serve as an accurate measure of its spreadability when applied in thin layers for additive manufacturing. This study further establishes a crucial connection between the intrinsic properties of individual particles and the collective behaviour of particles within the bulk material.

* Corresponding author.
E-mail address: M.Ghadiri@leeds.ac.uk (M. Ghadiri).
[1] *School of Mechanical and Power Engineering, Nanjing Tech University, Nanjing 211,816, China*
[2] *Janssen Pharmaceutical,Turnhoutseweg 30, B-2340 Beerse, Belgium*
[3] *Biophysics & Formulation, Novo Nordisk A/S, Novo Nordisk Park, DK-2760,Denmark*
[4] *School of Engineering, Newcastle University, Newcastle, NE1 7RU, UK*

https://doi.org/10.1016/j.powtec.2024.119471
Received 1 November 2023; Received in revised form 17 January 2024; Accepted 24 January 2024
Available online 28 January 2024

1. Introduction

In the realm of Additive Manufacturing (AM), especially employing the Binder Jet 3D printing technology, as exemplified by HP Metal Jet 3D printer [1], the utilization of fine and cohesive powders is commonplace. However, these powders present formidable challenges during the spreading process, where a powder heap is evenly spread onto a work surface using a blade or roller spreader to form a thin, uniform powder layer. This step is pivotal, as any inconsistencies like empty patches or uneven packing can detrimentally impact the quality of the final manufactured component [2,3]. The prediction of spreadability in this context is no simple task, owing to the diverse properties of powders and their sensitivity to environmental conditions. Nevertheless, such predictive insights are of paramount importance. It is worth noting that recent investigations work [2–9] have demonstrated that spreadability and flowability are distinct characteristics. Unfortunately, the dearth of commercial instruments designed to assess powder spreadability has impeded progress in this area. Consequently, a profound comprehension of the physical and mechanical attributes of powders that influence their spreadability within AM is invaluable for technological advancement and the incorporation of novel materials. In the absence of instruments for evaluating spreadability, traditional commercial or newly-developed tools for flowability evaluation are often employed to infer the spreadability of powders intended for AM. While spreadability and flowability are related bulk powder qualities, they differ in that flowability gauges resistance in naturally-developing shear bands, whereas spreadability concerns flow within confined spaces, heavily influenced by friction and transient jamming due to interactions with confining solid boundaries.

Recent research has endeavoured to characterise AM powder flowability to deduce spreadability [10–13]. For instance, Spierings et al. [10] utilised the Revolution Powder Analyzer (i.e. a rotating drum), to examine powder avalanche angles and surface fractals of atomised nickel and iron powders in selective laser melting (SLM). Similarly, Espiritu et al. [11] explored the flowability of IN625 and Ti6Al4V powders utilised in Laser powder bed fusion (LPBF) and electron beam melting (EBM), respectively, using dynamic repose angle and cohesive index from GranuDrum instrument. Their findings shed light on how atmospheric conditions (air/argon) and low-pressure environments impact flowability. Ruggi et al. [12] conducted shear tests on PA12 and PA6 powders with varying Sauter mean diameters at different temperatures. Their results indicated a notable deterioration in flowability at temperatures slightly below the polymer melting point. Zegzulka et al. [13] undertook an analysis of powder flowability using static and dynamic angles of repose, as well as the effective internal friction angle, employing tools such as the Ring Shear Tester RST-01, Brookfield PFT Powder Flow Tester and the shear cell unit of FT4 Powder rheometer. They also explored the effect of particle size and shape, using a diverse set of metal powders. Notably, there was inconsistency between results from different manufacturers' devices. However, their work utilised only a limited array of characterisation instruments and methods, rendering it insufficient for comprehensive powder spreadability inference [10–13]. There is lack of comprehensive characterisation of metal powders in Additive Manufacturing, both at the single particle and bulk powder levels, particularly for gas-atomised powders with surface burrs and bonded particles. In such cases, particle shape often varies with particle size [3]. Moreover, research on fine metal powders smaller than 15 μm in diameter remains scarce, owing to the challenges posed by cohesion and fluid medium drag. These finer powders are integral to binder jet 3D printing. Beyond experimental tests, some researchers [3–5,14] have endeavoured to directly model spreadability using the Discrete Element Method, establishing links between spreadability and the physical and mechanical properties of individual particles. For example, Xu et al. [4] revealed the influential role of interfacial surface energy, rolling friction coefficient of single particle as well as the roughness of the work surface on particle jamming in narrow gaps. Nonetheless, much work lies ahead, including the development of commercially available spreadability testing methods that assess powder flow behaviour [15].

Given the absence of such instruments, our current study delves into the single particle and bulk powder characterisation of two gas-atomized metal powders for AM, based on Binder Jet 3D printing technology. The single particle data are then used in numerical simulations of roller spreading by the Discrete Element Method, providing insights into differences between the powders based on their properties. Our single particle characterisation entails the determination of particle size and shape distributions, shape reconstruction, and interfacial surface energy/adhesion. Bulk characterisation involves the Ball Indentation Method at low consolidation stresses, dynamic (by Freeman FT4 rheometer) and quasi-static flow measurements (by Schulze shear cell), tap density, Hall Flow Meter and finally static and dynamic angle of repose measurements. Numerical characterisation of the spreading process encompasses studying particle flow patterns within the heap, as well as the packing fraction and segregation of the final spread layer. Our study not only supplies input data for DEM simulations, but also offers a comprehensive juxtaposition of bulk flow behaviour for two test powders across widely used instruments and the powder spreading process. Furthermore, it establishes a link between single particle attributes and bulk powder behaviour, encompassing flowability and spreadability. These findings hold potential for AI-based research into powder rheology.

2. Experimental characterisation of single particle and bulk powder

In this work, two distinct types of gas-atomised 316 L stainless steel powders are used: powder from Sandvik Osprey Ltd., Neath, UK, and Ancor powder manufactured by GKN Hoeganaes Corporation, Cinnaminson, NJ, USA. They are hereinafter simply referred to as Sandvik and Ancor powders, respectively. Initially a visual analysis of these gas-atomised metal powders is conducted utilising SEM images, as shown in Fig. 1. Both types predominantly exhibit a spherical shape; however, the particles from Sandvik powder exhibit distinctive attributes such as surface burrs, roughness and occasional non-spherical agglomerates. To ensure that the samples are representative and to minimise any potential influence of size segregation, the supplied powders are split using a Quantachrome Rotary Micro Riffler into batches that are sufficiently small, so they could be directly introduced into the characterisation tools. Subsequently, the requisite quantity of powder samples required for various characterisation techniques is selected from these divided samples. Notably, the precision and consistency of our splitting and sample preparation methodologies are validated by the remarkable reproducibility of particle size distribution (PSD) observed in two separate split samples, although this data is not presented here for the sake of brevity. The single particle characterisation work encompasses the analysis of particle size and shape distribution, reconstruction of particle shapes, and determination of interfacial surface energy. In tandem, a comprehensive assessment of bulk cohesion and flowability is conducted through the utilization of a variety of specialized instruments and tests (some are developed in-house), each serving to provide a more thorough understanding of the powders' behaviour at both individual particle and collective levels.

2.1. Single particle characterisation

2.1.1. Particle size and shape distribution

The analysis of particle size distribution (PSD) is carried out by using Morphologi G3 (Malvern Panalytical Ltd., Malvern, UK). This method is based on optical microscopy and automatic image analysis. The samples are dispersed onto a microscope slide using the dry dispersion unit of the instrument. About 3 mm^3 of each sample is dispersed using a pressure pulse of 3 barg with an injection time of 20 ms. At least 10,000 particles

are scanned for each sample. The cumulative number-based particle size distribution is shown in Fig. 2(a), where the particle size is referred to the area-equivalent circle diameter. Sandvik sample has a finer particle size distribution. The number-based D_{10}, D_{50} and D_{90} are 2.0 μm, 3.8 μm and 7.5 μm for Sandvik sample, and 2.3 μm, 5.6 μm and 13.3 μm for Ancor sample, respectively. Further analysis for both samples is carried in terms of shape distribution, expressed in circularity (the ratio of the particle area-equivalent circle circumference to its actual perimeter), which is the measure of closeness to a perfect circle. The cumulative shape distribution of both samples is shown in Fig. 2(b). A notable shape difference could be found for two samples. A lower circularity for Sandvik sample is found compared to Ancor sample. This is in-line with observations from SEM images, as shown in Fig. 1, where Sandvik powder has significantly more surface irregularities in terms of burrs, roughness and presence of agglomerates than that of Ancor powder.

2.1.2. Particle shape reconstruction

To reconstruct the shape of particles, a representative sample is dispersed using the dispersion unit of Morphologi G3. The sample quantity, dispersion pressure and injection time are set to ensure uniform dispersion and to mitigate particles settling over each other. Several images of dispersed particles are taken by SEM and analysed by ImageJ software. Based on image analysis, the number based D_{10}, D_{50} and D_{90} are 2 μm, 4 μm and 11 μm for Ancor powder, and 1.5 μm, 3.5 μm and 7 μm for Sandvik powder, respectively. These values are slightly different from the ones obtained from optical-based image analysis using Morphologi G3, as SEM images have a much better depth of field and are hence viewed as more accurate. Based on the equivalent circle diameter of the projected area at rest, approximately 1000 to 1500 particles for each sample are classified into different size classes. For each size class, 3–14 particles are randomly selected, and their shapes are approximated by a number of overlapping spheres of different sizes, as shown in Fig. 3, following the same method as described by Pasha et al. [16] and Nan et al. [3]. For each size class, different particle shapes are assumed to have the same number frequency, with the total frequency equal to the frequency of this size class. For example, for class I of Sandvik powder, 10 particles are selected, so each particle has a frequency of 4.6%. Fig. 3 shows that particle shape varies with particle size for each sample, i.e. smaller particles tend to be more spherical as compared to larger ones. This feature influences interlocking of particles under shear deformation and should be accounted for in realistic numerical simulations.

2.1.3. Interfacial surface energy

The interfacial surface energy is measured by using the Drop Test Method, following the published procedures [17]. In this work, approximately 8000–10,000 particles are scanned before the drop test, and around 4000–6000 particles are analysed after the drop test. The average impact velocity v and contact half time Δt are 3.5 m/s and 230 μs, respectively, determined by motion analysis using a high-speed camera video recording of the drop test. The interfacial surface energy is estimated as 4.98 mJ/m^2 for Sandvik particles and 9.68 mJ/m^2 for Ancor particles, based on a force balance between adhesion and detachment force [17]. The Cohesion number and Bond number of an individual particle with a characteristic size of D_{90} for both samples are summarised in Table 1. Bond number is the ratio of the maximum tensile force predicted by JKR theory to the particle weight (mg), and the cohesion number is the ratio of the adhesive work to the particle's gravitational potential energy with a characteristic height equal to particle radius, given as [18,19]:

$$Bo = \frac{1.5\pi\Gamma R}{mg} \tag{1}$$

$$Coh = \frac{1}{\rho g}\left(\frac{\Gamma^5}{E^2R^8}\right)^{1/3} \tag{2}$$

where E is the Young's modulus, ρ is the density, and R is the radius of particle with a diameter of D_{90} from the image analysis based on SEM in Section 2.1.2. Both Bond number and Cohesion number of Sandvik sample are slightly larger than that of Ancor sample.

2.2. Bulk powder characterisation

2.2.1. Dynamic flow assessment

The dynamic flow behaviour of Sandvik and Ancor samples is assessed using the FT4 powder rheometer following the standard test procedure described in [20–22]. In this work, the standard 25 ml glass container is used, and the distance between the blade tip and the surrounding cylindrical glass vessel wall is 0.75 mm. The resistance of a powder to flow along with the rotating blade motion, i.e. the work done

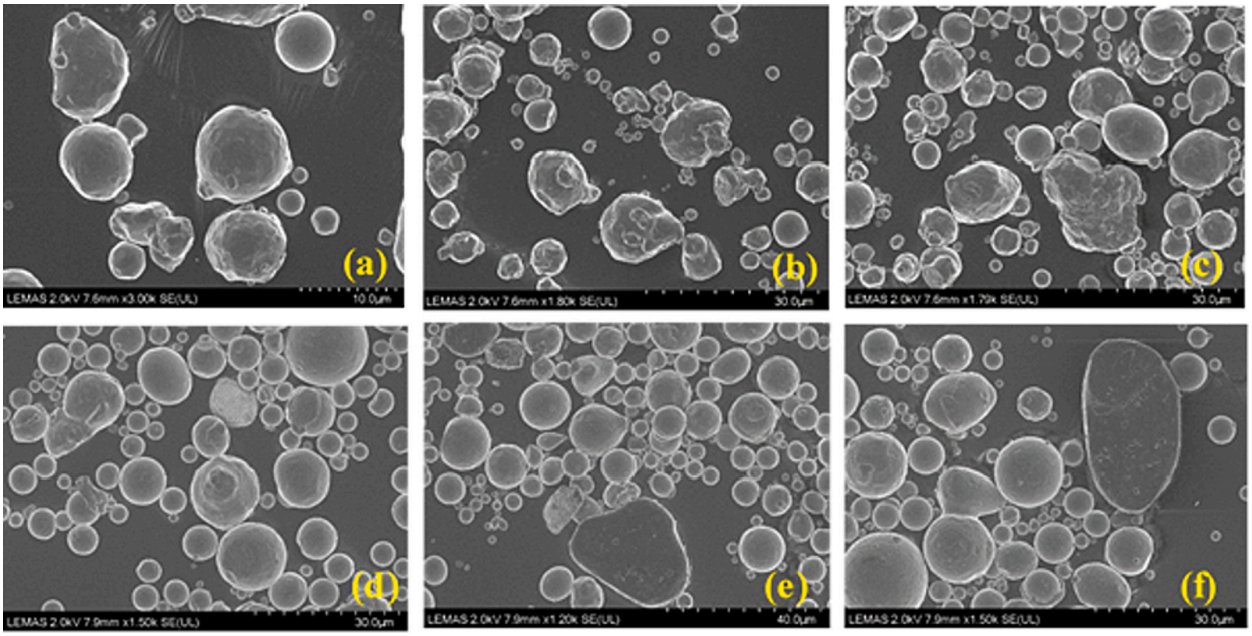

Fig. 1. SEM images of two distinct types of gas-atomised 316 L stainless steel powders: (a)-(c) Sandvik sample and (d)-(f) Ancor sample.

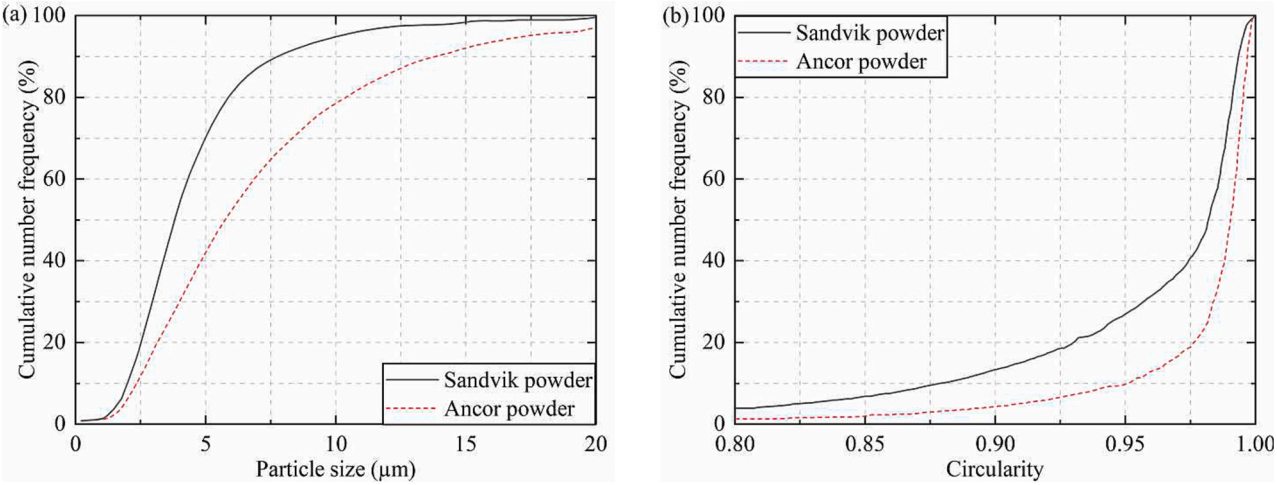

Fig. 2. Cumulative number frequency of (a) particle size distribution and (b) shape distribution for Sandvik and Ancor samples.

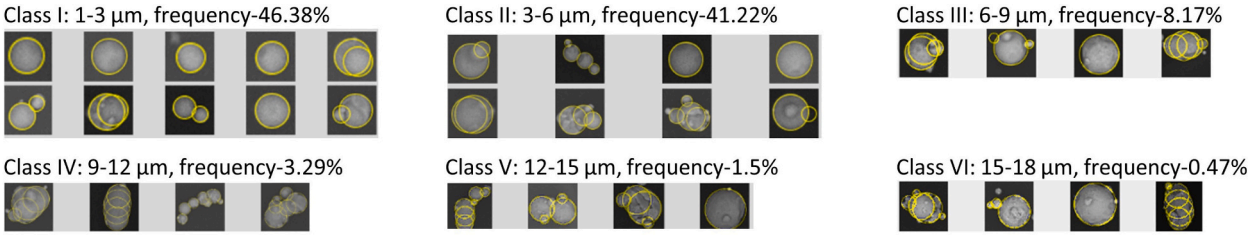

(a) Sandvik powder, for which 6 size classes with total 34 particles being randomly selected.

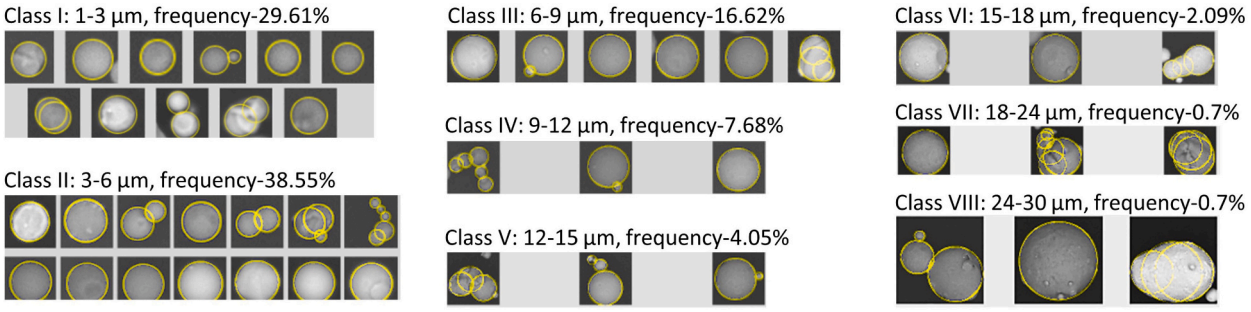

(b) Ancor powder, for which 8 size classes with total 46 particles being randomly selected.

Fig. 3. Reconstruction of particle shape for Sandvik and Ancor samples using overlapping sphere approach.

Table 1
Cohesive properties of Sandvik and Ancor samples.

Samples	Interfacial surface energy (mJ/m^2)	Bond number*	Cohesion number*
Sandvik	4.98	5848	0.0186
Ancor	9.68	4603	0.0168

* During the calculation, $E = 210$ GPa and $\rho = 7980$ kg/m^3 are used.

by the impeller, whilst moving downward and upward, is calculated and expressed as the specific downward flow energy (*SDFE*) and upward flow energy (*SUFE*), normalised by the mass of the powder that is being sheared [23]. The total specific downward flow energy at four impeller tip speeds of 100, 70, 40 and 10 mm/s is shown in Fig. 4.The average values of the *SDFE* and *SUFE* are compared in Table 2. For both samples, the specific total energy increases as the tip speed decreases from 100 mm/s to 10 mm/s. Furthermore, the SDFE for Sandvik sample is slightly higher compared to Ancor sample, suggesting more resistance to flow. However, the difference in *SUFE* is more pronounced between the two samples, with Sandvik sample having a higher average specific energy of 4.7 mJ/g compared to Ancor sample of 2.9 mJ/g.

2.2.2. *Quasi-static flow assessment*

The quasi-static flow behaviour of Sandvik and Ancor samples is assessed using Schulze Ring Shear Tester (RST-XS) with a 30 ml cell following the standard test procedure [24]. By plotting the unconfined yield strength σ_c, as a function of the major principal stress σ_1, the flow function coefficient, $ffc = \sigma_1/\sigma_c$ is evaluated, which is generally taken as an indicative index of powder flowability. The unconfined yield strength is directly related to bulk cohesion, so the flow function may be used as an indirect representation of bulk powder cohesion in response to the applied pre-consolidation load. The larger the value of the flow function coefficient, the more readily the powder flows. Jenike [25] introduced a powder flow classification as a guideline to the nature of a powder under certain conditions, i.e. $ffc < 1$ indicates not flowing, $ffc = 1$–2 for very cohesive flow, $ffc = 2$–4 for cohesive flow, $ffc = 4$–10 for easy flow, and

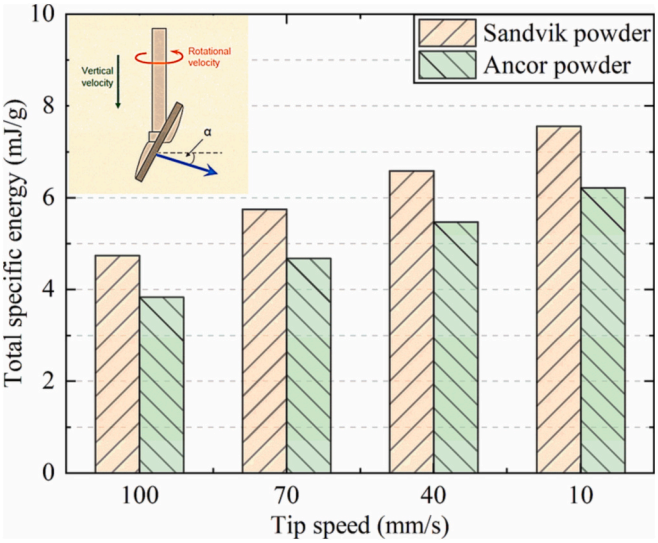

Fig. 4. Total specific energy obtained from the standard downward test of FT4 powder rheometer.

Table 2
Average flow energy of Sandvik and Ancor samples obtained from FT4 powder rheometer.

Samples	Specific Downward Flow Energy, *SDFE* (mJ/g)	Specific Upward Flow Energy, *SUFE* (mJ/g)
Sandvik	6.21	4.7
Ancor	5.13	2.9

ffc > 10 for free flow, as shown in Fig. 5(a).

In this work, the tests are carried out at four normal stresses (2, 4, 6 and 8 kPa) with 0.025 mm/min rotational shear velocity. The variation of the unconfined yield strength with major principal stress is shown in Fig. 5(a). Notable differences in the flow behaviour between Sandvik and Ancor samples prevail, with the latter showing relatively easy flowing behaviour (with *ffc* range between 2.99 and 7.37) compared to Sandvik sample (with *ffc* range between 1.47 and 3.39). Further analyses are carried out in terms of particle-particle friction referred to as internal angle of friction, as shown in Fig. 5(b). Sandvik sample exhibits a higher internal angle of friction at all normal stresses compared to Ancor sample. Furthermore, the internal angle of friction decreases with the increase in normal stress. Overall, Sandvik sample has a higher tendency for interlocking and higher friction compared to Ancor sample. The flow classification with respect to the flow function and internal angle of friction of both samples is given in Table 3. Sandvik powder is very cohesive - cohesive while Ancor powder is cohesive - easy flowing, depending on the normal stress.

2.2.3. Ball indentation method

Ball Indentation Method (BIM) [26–28] is used for assessing the flow resistance of cohesive powders, based on indentation test carried out on compacted powder beds. The bulk resistance of Sandvik and Ancor powders against plastic deformation, given as the ratio of the indentation load to the corresponding projected area of the impression, is determined following an established test procedure [24]. The loose powder is first sieved into the die by using a sieve with a mesh opening of approximately five times of the mean particle diameter. This procedure breaks cohesively-bonded clusters/agglomerates in the bulk on sieving and packs them uniformly with low stress into a cylindrical die, which is made of stainless steel and has an inner diameter of 20 mm. The sample is then pre-consolidated in the die by a stainless-steel piston under very low stresses prior to being subjected to indentation tests using the Instron 5566 machine (Instron Corp., USA). A high precision spherical glass ball of 2.38 mm diameter (Sigmund Lindner GmbH) is used as the indenter tip and is mounted on the loading head of the machine.

An initial investigation is carried out at different test conditions (i.e. indentation load and indenter size) to identify the optimal operation window for each sample. A characteristic load-displacement for Sandvik sample is shown in Fig. 6(a), along with the indentation impressions made on the surface of the packed powder bed, in which different indentation loads (5, 9, 15 and 23 mN) are applied with almost 0 kPa pre-consolidation stress. The calculated flow resistance values are plotted as a function indentation strain, as shown in Fig. 6(b). The flow resistance remains roughly constant above 9 mN indentation load for Sandvik sample, provided the penetration depth does not exceed the indenter radius (i.e. 50% strain). It is worth noting that at 5 mN indentation load, the strain is <10% and might not have enough indenter-particle contacts to cause plastic deformation. Based on these results, a ball indentation load of 15 mN is selected as the operation window for Sandvik sample. Using the same approach, a suitable ball indentation load for Ancor sample is found to be 5 mN. A ball indenter size of 4 mm is selected for both samples, the details of which are not shown here for brevity. Having identified these optimal process parameters, subsequent experiments are carried out at four different pre-

Table 3
Flow classification for Sandvik and Ancor samples as measured by the shear cell.

Samples	Flow function, *ffc*	Internal angle of friction, ϕ (°)	Flow classification
Sandvik	1.47–3.39	33.5–47.1	very cohesive – cohesive
Ancor	2.99–7.37	29.3–34.2	cohesive – easy flowing

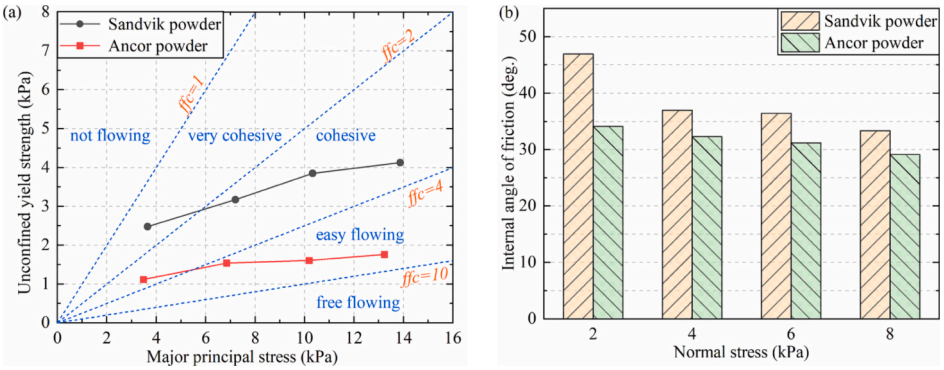

Fig. 5. Quasi-static flow assessment by shear cell for Sandvik and Ancor samples: (a) unconfined yield strength as a function of major principal stress; (b) internal angle of friction at four different normal stresses.

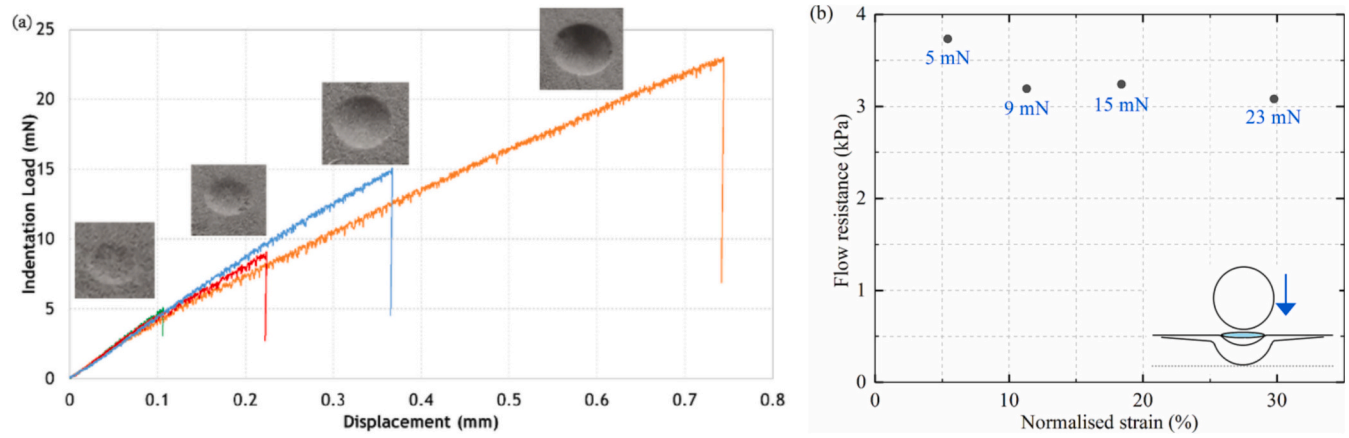

Fig. 6. Ball indentation experiment at different indentation loads (5, 9, 15 and 23 mN) with almost 0 kPa pre-consolidation stress: (a) load-displacement curve along with indentation impressions, and (b) flow resistance as a function of strain, where only the results of Sandvik sample are shown as an example.

consolidation stresses of 0, 0.5 and 1 kPa, respectively. The results are shown in Table 4. It is observed that the flow resistance values of Sandvik sample are at least twice higher compared to those of Ancor sample across all the pre-consolidation stresses tested. Therefore, BIM gives a large differentiation of yielding of the two samples, especially at low stresses corresponding to stresses experienced by powders during spreading process.

2.2.4. Tapped density

In this work, the tapped density tester series JV by Copley Scientific® is used to determine the tapped density ρ_{tapped} (mass/final volume) of the Sandvik and Ancor samples after a desired number of taps. A wide range of taps (from 4 to 1250 taps) is carried out for both samples. The magnified range with focus on lower number of taps is shown in Fig. 7. Sandvik sample has a lower tapped density (around 3.8 g/ml) compared to Ancor sample (around 4.9 g/ml). Both samples reach equilibrium after only a short number of taps. It is worth noting from Fig. 7(a) that a lower number of taps are required in the case of Ancor sample to reach equilibrium tapped density (around 10 taps) compared to Sandvik sample (around 16 taps), indicating that Ancor powder packs quicker. Further analysis in terms of compressibility ($(\rho_{tapped} - \rho_{bulk})/\rho_{tapped} \times 100$) and Hausner ratio ($\rho_{tapped}/\rho_{bulk}$) is also carried out. Ancor sample has a slightly higher compressibility index compared to Sandvik sample, as shown in Fig. 7(b). Meanwhile, the averaged Hausner ratio is 1.083 and 1.103 for Sandvik and Ancor powders, respectively. By definition, powders with a compressibility index of <10 and a Hausner ratio of <1.11 are deemed having excellent flow properties, and both Sandvik and Ancor powders fall within this category. This indicates that both the compressibility index and Hausner ratio are inadequate in distinguishing the flow characteristics of the two powder samples.

2.2.5. Static angle of repose

The angle of repose depends on many factors such as particle friction, cohesion shape, height of fall as well as operative errors. Nevertheless, it is perhaps the simplest test to perform and is widely used [29]. In this work, five measurements are carried out for each sample using a constant powder mass of 40 g. A comparison of static angle of repose between Sandvik and Ancor powders is given in Table 5. Sandvik sample exhibits a higher static angle of repose (around 51.3°) compared to that of Ancor sample (around 39.3°), which classifies them into poor and moderate flowing behaviour, respectively.

Table 4
Flow resistance as a function of pre-consolidation stress for Sandvik and Ancor samples.

Samples	Pre-consolidation stress (kPa)		
	0	0.5	1.0
Sandvik	2.94 kPa	3.25 kPa	3.86 kPa
Ancor	0.73 kPa	1.19 kPa	1.46 kPa

2.2.6. Dynamic angle of repose

Dynamic angle of repose experiments are carried out using GranuDrum (GranuTools® Awans, Belgium), following the test procedure described by Lumay et al. [30]. The drum is a short aluminium cylinder (more like a flat ring), sandwiched by two glass end walls. The internal diameter of the cylinder is 84 mm and the internal distance between the glass walls is 20 mm. The drum is loaded up to around half of its volume and is then rotated at five rotational speeds (2, 4, 6, 8 and 10 rpm) to acquire the flow profile. At each rotation speed, 20 images are taken with the built-in CCD camera. The position of free surface, i.e. air/powder interface, is determined by an edge detection algorithm. Using the fluctuations of the interface, the standard deviation is computed and referred as cohesive index. This parameter along with dynamic angle of repose are used for the comparison of flow behaviour between Sandvik and Ancor samples. All the measurements are taken at room temperature and 45% RH.

According to Fig. 8(a), the dynamic angle of repose for increasing rotation speed remains almost constant. Sandvik sample has a larger average dynamic angle of repose of 47.6° compared to Ancor sample having an average dynamic angle of repose of 35.5°. Furthermore, the Cohesive Index for increasing rotation speed is shown in Fig. 8(b). The average Cohesive Index of Sandvik sample is 62, which is almost three times of Ancor sample with an average value of 22. It should be noted that the Cohesive Index is a complex parameter as it is affected by many factors including bulk cohesion, particle shape, etc. There is lack of literature to provide an in-depth analysis, and therefore a systematic study to decouple the effect of the particle properties is needed for enhanced understanding.

2.2.7. Flow through orifice

Hall flow and Carney flow techniques are widely used in AM industry for assessing metal powder flowability and consistency between batches. They are both very similar in terms of principle of operation, which is based on the time taken by the powder to flow through an orifice. However, there are small differences in geometry of these devices, where the Hall flow test funnel has a smaller aperture compared to Carney flow funnel. The test procedure is according to ASTM B213 and ASTM B964 for Hall flow and Carney flow tests, respectively. Three repetitive measurements for Sandvik and Ancor samples are done using Hall flow tester with smaller aperture opening and using Carney flow tester with larger orifice opening. Both Sandvik and Ancor samples do

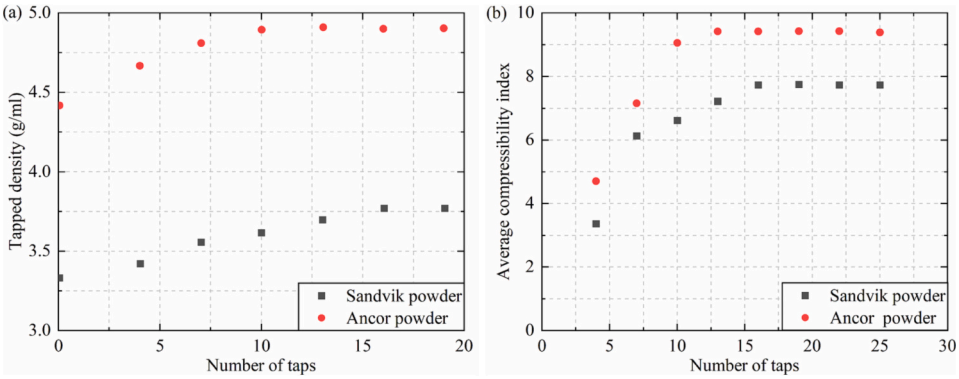

Fig. 7. Evolution of (a) tapped density and (b) compressibility index with number of taps for Sandvik and Ancor samples.

Table 5
Comparison of static angle of repose for Sandvik and Ancor samples.

Samples	Angle of repose	Classification
Sandvik	51.3°	poor flow
Ancor	39.3°	moderate flow

not flow through the orifice using either of these test methods, suggesting a very cohesive behaviour of the powder and invalidating the reliability of these methods to decipher any differences in flowability between the two samples.

3. Numerical characterisation of the spreading behaviour of powder

The spreading behaviour of Sandvik and Ancor samples by a roller is characterised by numerical simulations using Discrete Element Method. The simulations are conducted using Altair EDEM™ software package, and the interaction between particle and particle/wall is described by Hertz-Mindlin model with JKR theory, with more information referred to Appendix and Thornton [31]. The physical and mechanical properties of particles used in the simulations are based on the characterisation work done in Section 2.1, including size and shape distributions as well as the interfacial surface energy of the particles. The spreading process is analysed by assessing the bulk powder behaviour in the heap, i.e. flow pattern, and the quality of the thin spread layer after spreading.

3.1. Simulation conditions

Due to the limitation of computational power and memory capacity, simulating the process with the actual particle shape and size distributions is rather time-consuming, even with the use of the state-of-the-art GPUs. Therefore, the particle size in DEM simulations is scaled up by a factor of 10, i.e. all clumped spheres used to approximate the particle shape in Fig. 3 are scaled up by a factor of 10, and the particle shape distribution is the same as the ones shown in Fig. 3. Meanwhile, the particle Young's modulus is reduced by a factor of 1000. As the particles are cohesive, it is necessary to scale the interfacial surface energy accordingly to preserve the dynamics of the process. For this purpose, the scale law based on cohesion number (Eq. (2)) is used [19,32,33] and it is kept constant during scaling. The physical and mechanical properties of particles used in the numerical simulations are given in Table 6, where the density, Young's modulus, restitution coefficient, and friction coefficient are adopted from the work of Nan et al. [3]. In the simulations, the roller and base have the same material properties as the particles. The interaction parameters for particle-wall contact are the same as those for particle-particle contact.

The simulation system comprises a spreading roller and a rectangular base. The front and rear boundaries (in the Y direction) of the simulation domain are treated as periodic boundaries for particle flow, for which the effect of domain width on the particle flow is minimised. The diameter of the roller is 40 mm. Both the roller and base have the same width as the simulation domain in the Y direction, i.e. 10D, where D represents the characteristic scale used in the simulation system and is equal to number-based D_{90} of particles. To mitigate the bulk sliding of the particles, the base is made up of touching cylinders with diameter of D and axes along the Y direction, generating artificial roughness on the walls. The initial particle bed is prepared by using the poured packing method, where approximately 500,000 particles are generated. As the particle bed is generated, the roller spreader is placed at a specified position, forming a vertical gap of δ between the roller and base. As the spreading process begins, the roller moves along the X direction with a constant translational speed of U and rotates anti-clockwise with a constant angular speed of ω, by which the particles are spread onto the

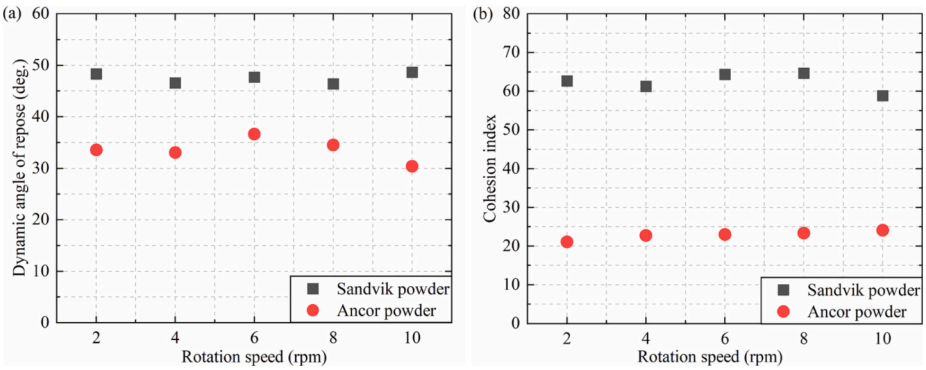

Fig. 8. Flowability of bulk powder measured by Granudrum as a function of rotation speed for Sandvik and Ancor samples: (a) dynamic angle of repose; (b) cohesion index.

Table 6
Physical and mechanical properties of particles used in the simulation.

Parameters	Sandvik powder	Ancor powder
Particle diameter[1], D_{90} (μm)	70	110
Particle density, ρ (kg/m^3)	7980	7980
Young's modulus[1], E (MPa)	210	210
Poisson's ratio, ν (−)	0.3	0.3
Friction coefficient[2], μ (−)	0.5	0.5
Restitution coefficient, e (−)	0.64	0.64
Interfacial surface energy[3], Γ (mJ/m^2)	12.5	24.3

[1] To speed up the simulation, each particle shown in Fig. 3 is scaled up from their original sizes by a factor of 10, and the Young's modulus is scaled down from its original value by a factor of 1000.

[2] Sliding friction coefficients for particle to roller interaction is modified to 0.38 and 0.44 for Sandvik and Ancor powders, respectively due to roller surface cross-hatch pattern, as characterised using the same method from Nan et al. [3].

[3] Due to the scaling of particle size and Young's modulus, the interfacial surface energy is scaled accordingly from their measured values (i.e. 9.68 mJ/m^2 for Ancor powder and 4.98 mJ/m^2 for Sandvik powders) by keeping cohesion number constant.

rough base. The vertical gap between the roller and base is scaled up with the same factor as the particle size, i.e. $\delta = 70$ μm used in actual process is scaled up to $\delta = 700$ μm used in the simulation. Two rotational speeds of roller (ω) are considered in this work, i.e. 4 and 12 rps, while its translational speed is kept at $U = 254$ mm/s in all cases.

3.2. Simulation results

3.2.1. Flow pattern

To better illustrate the particle dynamics in the heap, five cells around the roller are selected, and the trajectories of the particles in these cells are tracked. The averaged trajectories of the particles are shown in Figs. 9 and 10, where the abscissa is the relative position of the particle centre x with respect to the roller centre x_c. For the case of Sandvik powder, as shown in Fig. 9, the particles move in a very simple way with a short route, such as straight towards the rough base or down along the slope of the heap close to the roller surface. A slightly different behaviour is observed when the rotational speed of the roller is increased, where the particles in cells 2–5 (i.e. red, blue, black and orange colours) seem to be slightly lifted up as the roller is moved. However, the particles in these cells seem to follow the same path as particles in cell 1 (green) overall.

In the case of Ancor powder, as shown in Fig. 10, the averaged trajectory of the particles in the cells shows a distinct difference compared to that of Sandvik powder. The particles in cell 1 (green) follow the same trajectory as those of Sandvik powder, while particles in cell 2 and 3 (red and blue, respectively) are slightly lifted up but stay in a similar location in front of the roller. The extent of lifting increases by increasing the roller rotational speed. Particles in cell 4 (black) move down on the surface of the heap until they reach to the middle of the heap, but it is not clear whether they would remain in the middle of the heap, as longer simulations are required to confirm this. There is a likelihood that these particles would move further down the heap and once they reach closer to the rough base, they are spread by the roller. Particles in cell 5 (orange) have similar trajectory compared to cell 4 (black), but move closer to the heap surface and reach to the base of the heap. Once the particles move down the heap surface and reach the rough base, they end up getting spread onto the rough base without getting recirculated into the heap.

3.2.2. Spread layer

When the particle spreading is finished, a thin layer of particles is formed on the rough base. Good particle spreading means a dense and uniform spread layer, i.e. large packing fraction of particles and unvarying particle size distribution (PSD) along the spreading direction. If the PSD of the spread layer is different from that of the initial bulk particle bed, a segregation of particles is implied in the spreading process. Thus, the packing and segregation extent of particles within the spread layer are analysed here.

To calculate the local variation in the packing extent of particles in the spread layer, the spread layer is divided into a number of identical cells, with the same width as the base in the Y direction. The volume of each cell V_{cell} is calculated based on the average value of maximum position of the particles in Z direction in each cell. The packing fraction, η, is then calculated:

$$\eta = \frac{\sum V_p}{V_{cell}} \tag{3}$$

where V_p is the volume of individual particles in each cell. The variation of packing fraction of the spread layer for both powders is shown in Fig. 11. Although Sandvik powder is more cohesive (larger Bond number) and the particles are more irregularly-shaped compared to Ancor, its packing fraction is higher compared to Ancor powder for both rotational speeds of the roller. This behaviour is expected to be due to larger ratio of gap height to particle size D_{90} used for Sandvik powder. Increasing the rotational speed does not change the packing fraction in the case of Sandvik powder. In contrast, the packing fraction of particles in the spread layer of Ancor decreases as the rotational speed is increased.

In order to assess the segregation of particles in the spread layer, the spread layer is divided into five identical cells along the spreading di-

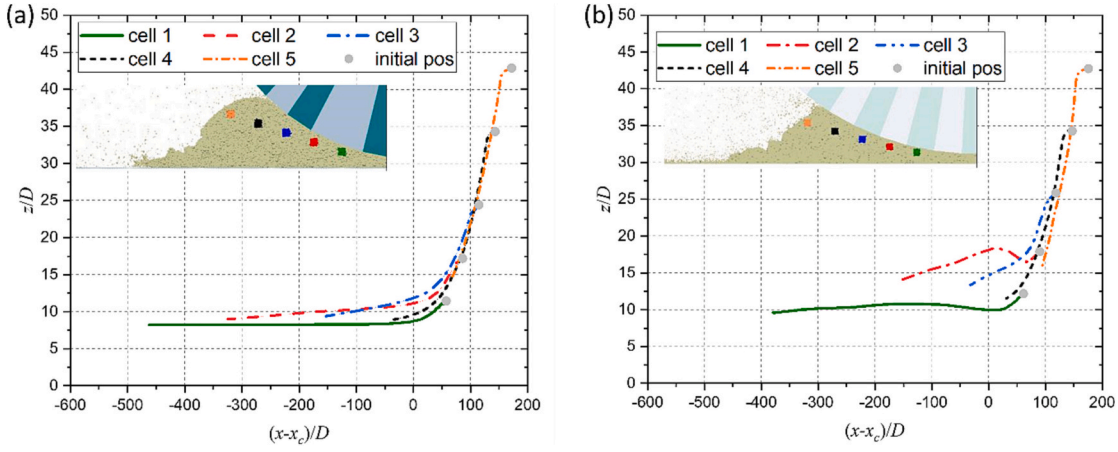

Fig. 9. Averaged trajectories of the particles in five tracking cells for Sandvik sample: (a) $\omega = 4$ rps and (b) $\omega = 12$ rps. Grey dots show the initial averaged position of the particles for each cell.

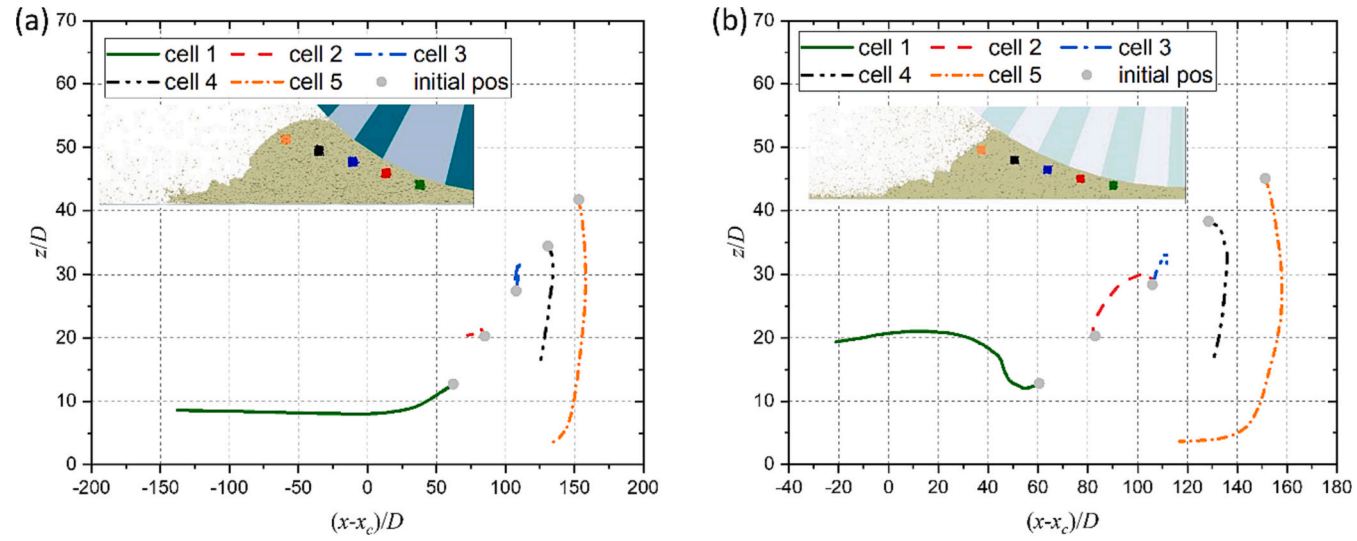

Fig. 10. Averaged trajectories of the particles in five tracking cells for Ancor sample: (a) $\omega = 4$ rps and (b) $\omega = 12$ rps. Grey dots show the initial averaged position of the particles for each cell.

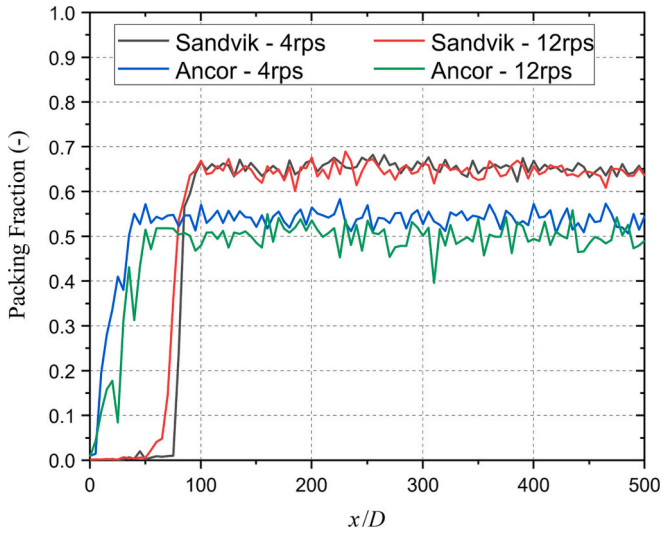

Fig. 11. Local variation of particles packing fraction along the spreading direction for Sandvik and Ancor samples.

rection (i.e. the X direction), with the same width as the base in the Y direction and the maximum height of spread layer in the Z direction. For each size class of particles, its number percentage x_{ji} in each cell is calculated, and the segregation index SI_j is calculated:

$$SI_j = \frac{\sigma_j}{x_{j0}} \tag{4}$$

where x_{j0} is the number percentage of particle size class j in the initial particle bed before spreading; σ_j is the deviation of x_{ji} from x_{j0} in all cells, given as:

$$\sigma_j{}^2 = \sum_{i=1}^{N} \frac{w_i \left(x_{ji} - x_{j0}\right)^2}{\sum_{i=1}^{N} w_i} \tag{5}$$

where w_i is the total number of all particles in cell i, and $N = 5$ is the number of cells. The segregation index SI_j equals to zero if the number percentage of particle j in every cell is identical to that of the initial particle bed.

The segregation index for different particle size classes of Sandvik and Ancor powder for both rotational speeds of the roller is shown in Fig. 12. It is evident that the segregation index of Sandvik powder is greater than that of the Ancor powder for all size classes. While the extent of segregation in the case of Sandvik powder changes slightly by increasing the rotational speed of the roller, this change is negligible. On the other hand, Ancor powder segregates more when the rotational speed is increased. Similar to the finding of Nan et al. [34], larger particles of Ancor segregate more compared to smaller particles as the spreading of larger particles is limited by the normalised gap height. The reason for the difference in the magnitude of the segregation between these two powders is not clear but this could be due to the particles being more irregularly-shaped for Sandvik powder compared to Ancor powder.

4. Discussions

The particles of Ancor 316 L powder have a larger interfacial surface energy. However, due to their larger average size, their granular Bond number and cohesion number is slightly smaller, resulting in lower

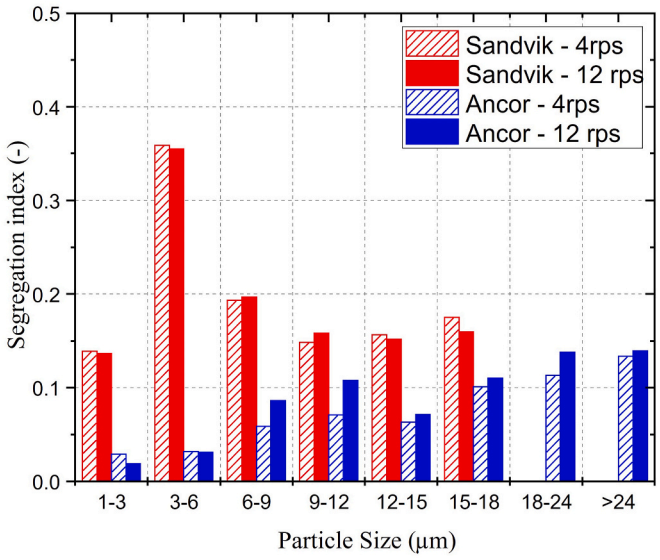

Fig. 12. Variation of the segregation index of spread layer with particle size class for Sandvik and Ancor samples.

cohesiveness when compared to the particles of Sandvik powder. The particles of Sandvik powder have more surface burrs, asperities and sintered agglomerates in comparison to those of Ancor. When comparing the flow resistance of the two samples, the Ball Indentation Method gives a clearer delineation, especially at lower stress levels similar to those experienced during powder spreading process. As determined by the Ball Indentation Method, the bulk flow resistance of Sandvik sample is at least twice as high as that of the Ancor sample.

The classification of flow behaviour yields contradictory results among various characterisation methods, as detailed in Table 7. For instance, Hall Flow and Carney Flow Testers reveal cohesive arching in the funnel, preventing powder flow for both samples, while the compressibility index and Hausner ratio suggest ease of flow behaviour for both samples. In contrast, the dynamic angle of repose is slightly lower than the static angle of repose, with a value of 47.6° and 35.5° for Sandvik and Ancor samples, respectively. Considering these findings, it is imperative to employ a well-suited set of tools for bulk flow characterisation when investigating flow-related issues and providing specific information for AM applications.

In the case of Sandvik powder, no circulation of powder within the heap, formed in front of the roller, is seen and this observation remains valid even when the rotational speed of the roller is increased. This might be due to the larger bulk cohesion and higher degree of departure from spherical shape, due to the presence of burrs and multiple particles stuck/sintered to each other. In the case of Ancor powder, a circulation of powder particles within the heap and more complex trajectory of particles is observed. This is consistent with the results of bulk powder flow characterisation using the commercial instruments discussed above, in which Ancor powder has a better flowability compared to Sandvik powder.

Surprisingly, the packing fraction of the final spread layer of the Sandvik powder is higher than that of the Ancor powder across the range of roller rotational speeds investigated in this study. Notably, the packing fraction of the spread layer of Sandvik powder remains constant, displaying no sensitivity to variations in roller rotational speed. In contrast, the packing fraction for the Ancor powder spread layer decreases as the rotational speed of the roller is increased. Interestingly, despite experiencing a more extensive recirculation within the heap, the Ancor powder exhibits a lower degree of segregation. These observations are in stark contrast to the qualitative results obtained through the bulk powder characterisation techniques discussed earlier.

It is worth noting that the simulations discussed earlier do not account for the influence of fluid medium drag (interstitial gas). However, as the printing chamber pressure must be slightly higher than the internal pressure of the printhead to prevent the binder from dripping out of the print head, the spreading process is in a gas-filled environment instead of a vacuum environment. The room atmosphere used in binder jetting, i.e. density of 1.2 kg/m^3 and a viscosity of 1.8 $\times$ 10^{-5} Pa·s, is considered here. Applying the same analytical approach as of Nan et al. [35], reveals that both Sandvik and Ancor powders are indeed responsive to the effects of the fluid medium and the gas flow induced by the roller action, as shown in Table 8.

Table 7
Flow classification as measured by various commercial tools.

Methods	Samples	Not flowing	Very cohesive	Cohesive	Easy flowing
Shear Cell assessment*	Sandvik	–	√	√	–
	Ancor	–	–	√	√
Compressibility index and Hausner ratio	Sandvik	–	–	–	√
	Ancor	–	–	–	√
Hall Flow Tester and Carney Flow Tester	Sandvik	√	–	–	–
	Ancor	√	–	–	–
Static angle of repose	Sandvik	Poor flowing (repose angle of 51°)			
	Ancor	Moderate flowing (repose angle of 39°)			

* Flow function coefficient and internal angle of friction are characterised, and the results depend on normal stress.

The Archimedes number is small for both samples due to their fine sizes, i.e. D_{10} = 1.5 and 2 μm as well as D_{90} = 7 and 11 μm for Sandvik and Ancor powders, respectively. Following the gas sensitivity index proposed by Guo et al. [36,37], it is evident that both samples are classified as sensitive to the presence of gas, the effect of which is more influential on Sandvik powder than it is on Ancor powder.

Additionally, the terminal velocities of particles in both samples are remarkably low. For instance, the terminal velocities of Sandvik particles with the characteristic sizes of D_{10}, D_{50} and D_{90} are 0.54, 2.96 and 11.79 mm/s, respectively. The ratio of the roller tip speed u_{tip} to the particle terminal velocity u_t could be used as a non-dimensional number to quantify the effects of gas flow induced by roller action on particle dynamics. Nan et al. [35] showed that the total volume of particles within the spread layer in the presence of fluid medium with $u_{tip}/u_t = 4.6$ was only half of that in vacuum (Fig. 9 in Ref. [35]). As shown in Table 8, in the case of Ancor sample, the ratio of u_{tip}/u_t is 783 for particle with a diameter of D_{10}, and it is 26 for a particle with diameter of D_{90}, which is much larger than the ones used in Nan et al. [35]. Thus, it is intuitively expected that partial fluidisation of particles would be induced by the roller action, and the spreadability is significantly affected by the presence of gas, especially for Sandvik sample.

It becomes clear that powder flowability does not provide a suitable or sufficient metric for assessing powder spreadability, especially in the context of Additive Manufacturing, where the thin spread layer is merely a few particle diameters thick. There is a need to develop a comprehensive regime map that takes into account particle characteristics (including size and shape distributions, density, friction, and adhesion) and spreading parameters (such as spreader geometry and size, spreading speed, gap distance, and the presence of a fluid medium). This regime map can help pinpoint the specific conditions under which the influence of these factors on spreadability becomes significant.

5. Conclusions

In this study, a thorough characterisation of two distinct types of gas-atomised metal powders used in Binder Jet 3D printing technology, denoted as the Sandvik and Ancor powder samples, has been conducted. The characterisation efforts encompass experimental assessments at the single-particle level, including particle size and shape, and interfacial surface energy, along with the evaluation of particle cohesion and bulk flowability. Additionally, numerical analysis has been conducted to investigate flow patterns and the quality of the final spread layer. The primary findings can be summarised as follows:

1) In comparison to the Ancor sample, Sandvik sample has a finer particle size distribution and a lower circularity, with notable surface burrs and roughness. Interestingly, for both powder samples, the particle shape varies with particle size. The particle shape is reconstructed by fitting overlapping spheres into the SEM-acquired images. A notable observation is that the apparent interfacial surface energy of Sandvik particles is smaller than that of Ancor (measuring 4.98 mJ/m^2 versus 9.68 mJ/m^2), yet their smaller size imparts greater cohesiveness, as indicated by the granular Bond Numbers of 1462 and 1151, respectively.
2) Bulk characterisation tests such as shear cell test and compressibility index yield conflicting results. The Ball Indentation Method emerges as a more discriminative technique, effectively distinguishing between the flow resistances exhibited by the two powders samples, particularly at low stress level experienced by the powders during an Additive Manufacturing spreading process.
3) Numerical characterisation of the spreading behaviour using the Distinct Element Method reveals that Ancor powder particles exhibit a more pronounced circulation pattern within the heap compared to Sandvik powder, consistent with the bulk powder characterisation

Table 8
Sensitivity parameters of Ancor and Sandvik samples to the presence of gas.

Parameters	Sandvik powder [1]			Ancor powder [1]			Formulations
	D_{10}	D_{50}	D_{90}	D_{10}	D_{50}	D_{90}	
Archimedes number	0.001	0.012	0.099	0.002	0.019	0.386	$Ar = \frac{\rho_f(\rho_p - \rho_f)gd^2}{\mu^2}$
Gas sensitivity index [2]	0.88	0.73	0.60	0.83	0.70	0.51	$\xi = 1\text{-}ln\zeta/ln\zeta_c \text{with} \zeta = Ar\frac{\rho_p}{\rho_f}\zeta_c = 9.56 \times 10^6$
Terminal velocity (mm/s)	0.54	2.96	11.79	0.97	3.86	28.92	$u_t = \frac{\mu Re_t}{\rho_f d} \text{with} \frac{4}{3}\frac{Ar}{Re_t^2} = C_d(Re_t)^2$ $C_d = 24(1 + 0.15Re^{0.687})/Re$ [38]
Non-dimensional number (u_{tip}/u_t) [3]	1392	256	64	783	196	26	–

[1] The particle size is number-based and taken from Section 2.1.2. The room atmosphere with a density of 1.2 kg/m^3 and a viscosity of 1.8×10^{-5} Pa·s is adopted here.
[2] The particles are gas-inert when $\xi \leq 0$ and gas-sensitive when $0 < \xi < 1$, In the gas-sensitive regime ($0 < \xi < 1$), the larger the value of the index ξ, the more sensitive the particles are to the presence of gas [36,37].
[3] The roller tip speed $u_{tip} = 0.756$ m/s is calculated based on a roller diameter of 40 mm, with a rotational speed of $\omega = 4$ rps and a translational speed of $U = 0.254$ mm/s.

results. However, Sandvik powder produces a final spread layer with greater density, while also experiencing more pronounced segregation.

These findings underscore the need to develop specialized tools tailored for characterising powder spreadability to meet the unique demands of additive manufacturing applications. Our study provides a comprehensive comparison of bulk flow behaviours across commonly used instruments, enriching our understanding of flowability and spreadability.

Furthermore, this research establishes a crucial connection between the intrinsic properties of individual particles and the collective behaviour of bulk particles, emphasising the necessity of a combined approach involving characterisation and DEM modelling for investigating flow-related issues and providing application-specific information for Additive Manufacturing applications.

CRediT authorship contribution statement

Wenguang Nan: Formal analysis, Investigation, Visualization, Writing – original draft, Writing – review & editing. **Mehrdad Pasha:** Formal analysis, Investigation, Visualization. **Umair Zafar:** Formal analysis, Investigation, Visualization. **Sadegh Nadimi:** Formal analysis, Investigation. **Wei Pin Goh:** Investigation. **Mojtaba Ghadiri:** Conceptualization, Supervision, Writing – review & editing.

Declaration of competing interest

The authors declare that they have no known competing financial interests or personal relationships that could have appeared to influence the work reported in this paper.

Data availability

Data will be made available on request.

Acknowledgments

The authors are grateful for the support of Messrs. Ali Emamjomeh, Dani Gonzalez and Fernando Juan at Hewlett Packard (HP) 3D Printing and Digital Manufacturing Center of Excellence, Barcelona, Spain, and Vladek Kasperchik and Pavan Suri, IJPL R&D, Corvallis, Oregon, USA, for their helpful discussion and suggestions.

Appendix A. Appendix

Table A1
Summary of the models of normal and tangential contact forces in DEM simulation.

Interaction force	Formulations
Normal force	$\boldsymbol{F}_{en} = \left(\frac{4E^*a^3}{3R^*} - \sqrt{8\pi\Gamma E^* a^3}\right)\boldsymbol{n}$ (A1)
	$\boldsymbol{F}_{dn} = -2\sqrt{\frac{5}{6}}\beta_c\sqrt{S_n m^*}\boldsymbol{V}_n^{rel}$ with $S_n = 2E^*\sqrt{R^*\delta_n}$
	$\boldsymbol{F}_n = \boldsymbol{F}_{en} + \boldsymbol{F}_{dn}$
Tangential force	$\boldsymbol{F}_{et} = -S_t\delta_t\boldsymbol{t}$ with $S_t = 8G^*\sqrt{R^*\delta_n}$ (A2)
	$\boldsymbol{F}_{dt} = -2\sqrt{\frac{5}{6}}\beta_c\sqrt{S_t m^*}\boldsymbol{V}_t^{rel}$
	$\boldsymbol{F}_t = \begin{cases} \boldsymbol{F}_{et} + \boldsymbol{F}_{dt} & if \lvert\boldsymbol{F}_{et}\rvert \leq \mu\lvert\boldsymbol{F}_{en}\rvert \\ -\mu\lvert\boldsymbol{F}_{en}\rvert\boldsymbol{t} & if \lvert\boldsymbol{F}_{et}\rvert > \mu\lvert\boldsymbol{F}_{en}\rvert \end{cases}$
Variables	E^* and G^* are the equivalent Young's modulus and shear modulus, respectively; a is the contact radius; R^* and m^* are the equivalent radius and mass, respectively; Γ is the interfacial surface energy; $\boldsymbol{n}$ and $\boldsymbol{t}$ are the unit vectors in the normal and tangential directions, respectively; β_c is the damping constant; δ_n and δ_t are the overlaps in the normal and tangential directions, respectively; $\boldsymbol{V}_n^{rel}$ and $\boldsymbol{V}_t^{rel}$ are the normal and tangential components of the relative velocity at the contact point, respectively.

References

[1] https://www.hp.com/us-en/printers/3d-printers/products/metal-jet.html.
[2] M. Ghadiri, M. Pasha, W.G. Nan, C. Hare, V. Vivacqua, U. Zafar, S. Nezamabadi, A. Lopez, M. Pasha, S. Nadimi, Cohesive powder flow: trends and challenges in characterisation and analysis, Kona Powder Part. J. 37 (2020) 3–18.

[3] W. Nan, M. Pasha, T. Bonakdar, A. Lopez, U. Zafar, S. Nadimi, M. Ghadiri, Jamming during particle spreading in additive manufacturing, Powder Technol. 338 (2018) 253–262.
[4] R. Xu, W. Nan, Analysis of the metrics and mechanism of powder spreadability in powder-based additive manufacturing, Addit. Manuf. 71 (2023).
[5] S. Yim, H. Bian, K. Aoyagi, K. Yamanaka, A. Chiba, Spreading behavior of Ti 48Al 2Cr 2Nb powders in powder bed fusion additive manufacturing process: experimental and discrete element method study, Addit. Manuf. 49 (2022).
[6] C. Vakifahmetoglu, B. Hasdemir, L. Biasetto, Spreadability of metal powders for laser-powder bed fusion via simple image processing steps, Materials (Basel) 15 (2021).
[7] M. Mehrabi, J. Gardy, F.A. Talebi, A. Farshchi, A. Hassanpour, A.E. Bayly, An investigation of the effect of powder flowability on the powder spreading in additive manufacturing, Powder Technol. 413 (2023).
[8] M. Lupo, S.Z. Ajabshir, D. Sofia, D. Barletta, M. Poletto, Experimental metrics of the powder layer quality in the selective laser sintering process, Powder Technol. 419 (2023).
[9] H. Salehi, J. Cummins, E. Gallino, V. Garg, T. Deng, A. Hassanpour, M. Bradley, Optimising spread-layer quality in powder additive manufacturing: assessing packing fraction and segregation tendency, Processes 11 (2023).
[10] A.B. Spierings, M. Voegtlin, T. Bauer, K. Wegener, Powder flowability characterisation methodology for powder-bed-based metal additive manufacturing, Prog. in Addi. Manufac. 1 (2016) 9–20.
[11] E.R.L. Espiritu, A. Kumar, A. Nommeots-Nomm, J.A.M. Lerma, M. Brochu, Investigation of the rotating drum technique to characterise powder flow in controlled and low pressure environments, Powder Technol. 366 (2020) 925–937.
[12] D. Ruggi, M. Lupo, D. Sofia, C. Barrès, D. Barletta, M. Poletto, Flow properties of polymeric powders for selective laser sintering, Powder Technol. 370 (2020) 288–297.
[13] J. Zegzulka, D. Gelnar, L. Jezerska, R. Prokes, J. Rozbroj, Characterization and flowability methods for metal powders, Sci. Rep. 10 (2020) 21004.
[14] Y. He, A. Hassanpour, A.E. Bayly, Linking particle properties to layer characteristics: discrete element modelling of cohesive fine powder spreading in additive manufacturing, Addit. Manuf. 36 (2020) 101685.
[15] M. Ahmed, M. Pasha, W.G. Nan, M. Ghadiri, A simple method for assessing powder spreadability for additive manufacturing, Powder Technol. 367 (2020) 671–679.
[16] M. Pasha, C. Hare, M. Ghadiri, A. Gunadi, P.M. Piccione, Effect of particle shape on flow in discrete element method simulation of a rotary batch seed coater, Powder Technol. 296 (2016) 29–36.
[17] U. Zafar, C. Hare, A. Hassanpour, M. Ghadiri, Drop test: a new method to measure the particle adhesion force, Powder Technol. 264 (2014) 236–241.
[18] X. Chen, J.A. Elliott, On the scaling law of JKR contact model for coarse-grained cohesive particles, Chem. Eng. Sci. 115906 (2020).
[19] M.A. Behjani, N. Rahmanian, N. Fardina, bt Abdul Ghani, A. Hassanpour, An investigation on process of seeded granulation in a continuous drum granulator using DEM, Adv. Powder Technol. vol. 28 (2017) 2456–2464.
[20] R. Freeman, Measuring the flow properties of consolidated, conditioned and aerated powders — a comparative study using a powder rheometer and a rotational shear cell, Powder Technol. 174 (2007) 25–33.
[21] C. Hare, U. Zafar, M. Ghadiri, T. Freeman, J. Clayton, M.J. Murtagh, Analysis of the dynamics of the FT4 powder rheometer, Powder Technol. 285 (2015) 123–127.
[22] W.G. Nan, M. Ghadiri, Y.S. Wang, Analysis of powder rheometry of FT4: effect of particle shape, Chem. Eng. Sci. 173 (2017) 374–383.
[23] M. Pasha, N.L. Hekiem, X. Jia, M. Ghadiri, Prediction of flowability of cohesive powder mixtures at high strain rate conditions by discrete element method, Powder Technol. 372 (2020) 59–67.
[24] D. Schulze, Powders and Bulk Solids Behavior, Characterization, Storage and Flow, Springer, Verlag Berlin Heidelberg, 2007.
[25] A.W.J.B.N. Jenike, Utah State University, Storage and Flow of Solids, 1964.
[26] A. Hassanpour, M. Ghadiri, Characterisation of Flowability of loosely compacted cohesive powders by indentation, Part. Part. Syst. Charact. 24 (2007) 117–123.
[27] U. Zafar, C. Hare, A. Hassanpour, M. Ghadiri, Ball indentation on powder beds for assessing powder flowability: analysis of operation window, Powder Technol. 310 (2017) 300–306.
[28] M. Pasha, C. Hare, A. Hassanpour, M. Ghadiri, Analysis of ball indentation on cohesive powder beds using distinct element modelling, Powder Technol. 233 (2013) 80–90.
[29] D. Geldart, E.C. Abdullah, A. Hassanpour, L.C. Nwoke, I. Wouters, Characterization of powder flowability using measurement of angle of repose, China Particuol. 4 (2006) 104–107.
[30] G. Lumay, F. Boschini, K. Traina, S. Bontempi, J.C. Remy, R. Cloots, N. Vandewalle, Measuring the flowing properties of powders and grains, Powder Technol. 224 (2012) 19–27.
[31] C. Thornton, Granular Dynamics, Contact Mechanics and Particle System Simulations, Springer, New York, 2015.
[32] J. Hærvig, U. Kleinhans, C. Wieland, H. Spliethoff, A.L. Jensen, K. Sørensen, T. J. Condra, On the adhesive JKR contact and rolling models for reduced particle stiffness discrete element simulations, Powder Technol. 319 (2017) 472–482.
[33] K. Washino, E.L. Chan, T.J.P.T. Tanaka, DEM with attraction forces using reduced particle stiffness, Powder Technol. 325 (2018) 202–208.
[34] W.G. Nan, M. Pasha, M. Ghadiri, Numerical simulation of particle flow and segregation during roller spreading process in additive manufacturing, Powder Technol. 364 (2020) 811–821.
[35] W.G. Nan, M. Pasha, M. Ghadiri, Effect of gas-particle interaction on roller spreading process in additive manufacturing, Powder Technol. 372 (2020) 466–476.
[36] Y. Guo, C.Y. Wu, K.D. Kafui, C. Thornton, 3D DEM/CFD analysis of size-induced segregation during die filling, Powder Technol. 206 (2011) 177–188.
[37] Y. Guo, C.Y. Wu, C. Thornton, The effects of air and particle density difference on segregation of powder mixtures during die filling, Chem. Eng. Sci. 66 (2011) 661–673.
[38] D. Gidaspow, Multiphase Flow and Fluidization: Continuum and Kinetic Theory Descriptions, Academic press, 1994.